Janus Particles at Walls Modified With Tethered Chains.

4 AUTHORS, INCLUDING:

Thorsten Pöschel

Friedrich-Alexander-University of Erlangen-Nü…

214 PUBLICATIONS   **3,621** CITATIONS

SEE PROFILE

Janus Particles at Walls Modified with Tethered Chains

M. Borówko,[†] T. Pöschel,[‡] S. Sokołowski,*[,†,‡] and T. Staszewski[†]

[†]Department for the Modeling of Physico-Chemical Processes, Maria Curie-Skłodowska University, 20-031 Lublin, Poland
[‡]Institute for Multiscale Simulations, Friedrich-Alexander-Universität Erlangen-Nürnberg, D-91052 Erlangen, Germany

Ⓢ *Supporting Information*

ABSTRACT: We investigate the structure and adsorption of amphiphilic molecules at planar walls modified by tethered chain molecules using density functional theory. The molecules are modeled as spheres composed of a hydrophilic and hydrophobic part. The pinned chains are treated as tangentially jointed spheres that can interact with fluid molecules via orientation-dependent forces. Our density functional approach involves fundamental measure theory, thermodynamic perturbation theory for chains, and a mean-field approximation for describing the anisotropic interactions. We study the adsorption of the particles, focusing on the competition between the external field (due to the surface and due to attached chain molecules) and the interaction-induced ordering phenomena.
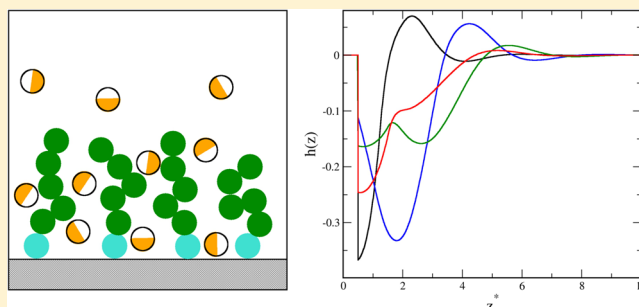
■ INTRODUCTION

The term "Janus particles" was introduced by Casagrande[1] to describe glass spheres coated in a special manner that one of the hemispheres was hydrophilic and the other one hydrophobic. Over the past two decades, Janus particles have drawn widespread attention in different fields of nanoscience.[2−12] However, a model of Janus particles can also be viewed as a coarse-grained model of real amphiphilic molecules[13−17] that are generally composed of hydrophilic and hydrophobic parts. The coarse-graining treats complex molecules as a sphere with anisotropic surface properties. Despite this simplification, which completely neglects several factors, such as relative size of different groups, the model is capable of describing the formation of bilayers, vesicles, and micelles.[18,19] The presence of hydropholic and hydrophobic ingredients yields a large variety of self-assembled structures on different length scales. These range from molecular size micelles to mesoscopic membranes, bicontinuous foams, and lamellar phases.[20−25]

One of the first simple theoretical models of Janus particles was introduced by Tarazona et al.[26] There exist also other models for Janus particles,[27−29] which are, in fact, similar to the model of Tarazona and co-workers.[26] One should also mention here about the "patchy-particle" model that has been proposed by Kern and Frenkel[30] and studied by Sciortino et al.[31] The patchy-particle model involves localized surface areas exerting homogeneous attractive forces, whereby the core is impenetrable. A graphical comparison of the models of Tarazona et al.[26] and Kern and Frenkel[30] has been given by Rosenthal.[18]

A recently published paper by Rosenthal and Klapp[32] employed the model of Tarazona et al.[26] to develop a density functional approach for describing amphiphilic molecules at planar walls and inside slit-like pores. The proposed approach involves fundamental measure theory combined with a mean-

field approximation for the anisotropic interaction. Considering neutral, hydrophilic, and hydrophobic walls, they focused on the problem how a competition between the surface field and the interparticle interaction induces ordering phenomena. In subsequent works, Klapp and co-workers[19,33] applied molecular dynamics simulations to investigate the structure formation of amphiphilic Janus particles in the bulk phase and in slit-like pores. The results for confined fluid were also compared with predictions of the density functional approach. Note that refs 18, 19, and 33 also contain a detailed description of the simulation methods.

In recent years, investigations of polymer films on solid surfaces have become one of the most rapidly growing research area in physics, chemistry, and material science. The reason for such sustained growth is due to the availability of a wealth of fundamentally interesting information in thermodynamics and kinetics, such as long- and short-range forces, interfacial interactions, flows, and instability phenomena.[34−38] Moreover, polymer thin films are widely used as an industrial commodity in coatings and lubricants, and they have become an integral part of the development process in several modern technological applications.[39−43]

In our previous works, we have intensively studied several aspects of adsorption of fluids on surfaces covered by tethered layers. Among others, we considered how tethered layers influence the surface-phase transitions in the case of adsorption on a single wall, and in pores with chemically modified walls,[44−48] we studied how the solvation force between two planar surfaces is influenced by their chemical modifications[49]

and considered how chemical modification of surfaces alters selectivity of adsorption of a binary mixture and the chromatographic separation process.[50,51] In our calculations, we used a version of the density functional that has been based on a combination of the fundamental measure approach and perturbation theory of chain's connectivity of Wertheim. In this work, we combine the theory outlined in refs 44−48 with the theory of Klapp et al.[18,19,33] to study adsorption of Janus-like particles on surfaces covered by tethered layers. In particular, we investigate how the presence of the preadsorbed layer and the interactions between segments and fluid particles influence the structure of the fluid at the wall.

■ MODEL AND THEORY

The model of the system under study is shown in Figure 1. We consider fluid of Janus particles in contact with a surface
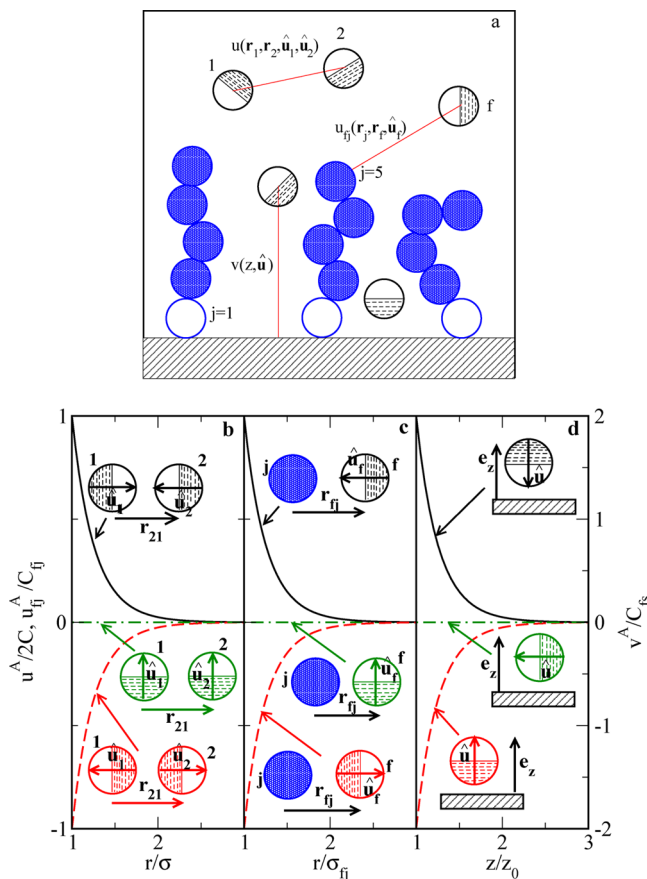
Figure 1. (a) Schematic representation of the system under study. Open circles are pinned ($j = 1$) segments. Filled circles are free segments. Hatched parts of the fluid particles indicate hydrophobic (attractive) hemispheres and open parts hydrophilic (repulsive) hemispheres. The interaction potentials between particular spherical species are marked by thin solid (red) lines. Parts (b−d) illustrate the fluid−fluid (part b), fluid−segment (part c), and fluid−wall (part b) orientation-dependent interaction potentials for three selected orientations of fluid molecules.

covered by brush molecules. The model of Janus molecules is the same as used in previous publications.[18,26,32,33] The fluid particles are represented by spheres with an internal degree of freedom, that is, a unit vector, $\hat{\mathbf{u}}_i$, pointing from the hydrophobic (attractive) to the hydrophilic (repulsive) hemisphere of each particle i.

The pair interaction between two Janus particles splits into a hard-sphere (HS) repulsion and an effective, solvent-mediated anisotropic pair interaction (A)

$$u(\mathbf{r}_1, \mathbf{r}_2, \hat{\mathbf{u}}_1, \hat{\mathbf{u}}_2) = u^{HS}(r_{12}) + u^{A}(\mathbf{r}_{12}, \hat{\mathbf{u}}_1, \hat{\mathbf{u}}_2) \tag{1}$$

where $\mathbf{r}_{12} = \mathbf{r}_1 - \mathbf{r}_2$, $r_{12} = |\mathbf{r}_{12}|$

$$u^{HS}(r_{12}) = \begin{cases} \infty, & r_{12} < \sigma \\ 0, & r_{12} \geq \sigma \end{cases} \tag{2}$$

and where σ is the hard-sphere diameter. The anisotropic part of the potential is given by

$$u^{A}(\mathbf{r}_{12}, \hat{\mathbf{u}}_1, \hat{\mathbf{u}}_2) = U(r_{12})(\hat{\mathbf{u}}_1 - \hat{\mathbf{u}}_2)\cdot\hat{\mathbf{r}}_{21} \tag{3}$$

In the above $\hat{\mathbf{r}}_{21} = \mathbf{r}_{21}/|\mathbf{r}_{21}|$ and

$$U(r_{12}) = \begin{cases} 0, & r_{12} < \sigma \\ C \exp[-\lambda(r_{12} - \sigma)]/r_{12}, & r_{12} \geq \sigma \end{cases} \tag{4}$$

In the above, C and λ are the energy and the size parameters of the Yukawa potential 4, respectively. The shape of the potential 1 for three selected orientations of the interacting particles is displayed in Figure 1. In the case of a solid line, the scalar product $(\hat{\mathbf{u}}_1 - \hat{\mathbf{u}}_2)\cdot\hat{\mathbf{r}}_{21} = 2$, and the anisotropic interaction $u^{A}(\mathbf{r}_{12}, \hat{\mathbf{u}}_1, \hat{\mathbf{u}}_2)$ is repulsive. For the dash-dotted line $(\hat{\mathbf{u}}_1 - \hat{\mathbf{u}}_2)\cdot\hat{\mathbf{r}}_{21} = 0$, while for the dotted line $(\hat{\mathbf{u}}_1 - \hat{\mathbf{u}}_2)\cdot\hat{\mathbf{r}}_{21} = -2$ and the potential $u^{A}(\mathbf{r}_{12}, \hat{\mathbf{u}}_1, \hat{\mathbf{u}}_2)$ is attractive (cf. Figure 1b).

The interaction of a fluid molecule with a bare solid surface is described by[18,32]

$$v(z, \hat{\mathbf{u}}) = v^{HW}(z) + v^{A}(z)(-\hat{\mathbf{u}}\cdot\hat{\mathbf{e}}_z) \tag{5}$$

where

$$v^{HW}(z) = \begin{cases} \infty, & z < \sigma/2 \\ 0, & z \geq \sigma/2 \end{cases} \tag{6}$$

is the hard-wall part of the potential; $\hat{\mathbf{e}}_z$ is the unit vector along the axis OZ, perpendicular to the surface; and the anisotropic potential is

$$v^{A}(z) = \begin{cases} 0, & z < \sigma/2 \\ C_{fs} \exp[-\lambda_{fs}(z - \sigma/2)]/z, & z > \sigma/2 \end{cases} \tag{7}$$

In the above, C_{fs} and λ_{fs} are the potential parameters. The plots of $v^{A}(z)$ for three selected orientations of fluid molecules are displayed in Figure 1d.

The surface is covered by preadsorbed chain molecules. Similarly as in previous works,[44−48] the chains are represented by tangentially jointed M spherical beads of the same diameter, σ_c. The chain connectivity is enforced by the bonding potential between nearest-neighbor segments, V_b. This potential satisfies the equation[52]

$$\exp[-\beta V_b(\mathbf{R})] = \prod_{j=1}^{M-1} \delta(|\mathbf{r}_j - \mathbf{r}_{j+1}| - \sigma_c)/4\pi\sigma_c \tag{8}$$

where $\beta = 1/kT$ and $\mathbf{R} = (\mathbf{r}_1, \mathbf{r}_2, ..., \mathbf{r}_M)$ is a vector specifying the positions of all the segments.

Each chain molecule contains one surface-binding segment, located at its end (and indexed as $j = 1$), that interacts with the wall via the potential

$$\exp[-\beta v_{s1}(z)] = \mathcal{W}\delta(z - \sigma_c/2) \tag{9}$$

where $\mathcal{W}$ is a constant. This potential implies that the surface-binding segments lie always at the distance $z = \sigma_c/2$ from the surface. The remaining segments of the grafted molecules ($j = 2, 3, ..., M$) are "neutral" with respect to the surface; i.e., they interact with the surface via a hard-wall potential

$$v_{sj}(z) = \begin{cases} \infty, & z < \sigma_c/2 \\ 0, & z \geq \sigma_c/2 \end{cases} \qquad (10)$$

The interactions between the segments of chains, $u_{ss}(r)$, are modeled by hard-sphere potentials

$$u_{ss}(r) = \begin{cases} \infty, & r < \sigma_c \\ 0, & r \geq \sigma_c \end{cases} \qquad (11)$$

We allow for anisotropy in the interaction between a fluid particle and the segment j

$$u_{fj}(\mathbf{r}_f, \mathbf{r}_j, \hat{\mathbf{u}}_f) = u_{fj}^{HS}(r_{fj}) + u_{fj}^{A}(\mathbf{r}_{fj}, \hat{\mathbf{u}}_f) \qquad (12)$$

where $\mathbf{r}_{fj} = \mathbf{r}_f - \mathbf{r}_j$ and

$$u_{fj}^{HS}(r_{fj}) = \begin{cases} \infty, & r < \sigma_{fj} \\ 0, & r \geq \sigma_{fj} \end{cases} \qquad (13)$$

$u_{fj}^{A}(\mathbf{r}_{fj}, \hat{\mathbf{u}}_f) = U_{fj}(r_{fj})(\hat{\mathbf{r}}_{fj} \cdot \hat{\mathbf{u}}_f)$, $\hat{\mathbf{r}}_{fj} = \mathbf{r}_{fj}/|\mathbf{r}_{fj}|$, and

$$U_{fj}(r_{fj}) = \begin{cases} 0, & r < \sigma_{fj} \\ C_{fj}\exp[-\lambda_{fj}(r - \sigma_{fj})]/r_{fj}, & r \geq \sigma_{fj} \end{cases} \qquad (14)$$

In the above, C_{fj} and λ_{fj} are the parameters, and $\sigma_{fj} = (\sigma + \sigma_c)/2$. Figure 1c illustrates the behavior of the anisotropic part of the fluid−segment potential for three selected orientations of fluid particles.

To proceed, we introduce the notation, $\rho^{(c)}(\mathbf{R})$ and $\rho(\mathbf{r}, \hat{\mathbf{u}}_f)$, for the density distribution of chains and of fluid species, respectively. The theory is constructed in terms of $\rho(\mathbf{r}, \hat{\mathbf{u}}_f)$, the density of particular segments of chains, $\rho_{sj}(z)$, and the total segment density of chains, $\rho_s(z)$. The densities $\rho_{sj}(z)$ and $\rho_s(z)$ are defined via commonly used relations; see refs 44−48 and 52.

$$\rho_s(\mathbf{r}) = \sum_{j=1}^{M} \rho_{sj}(\mathbf{r}) = \sum_{j=1}^{M} \int d\mathbf{R}\delta(\mathbf{r}_j - \mathbf{r})\rho^{(c)}(\mathbf{R}) \qquad (15)$$

In the system under study, the local densities of segments are only the functions of the distance from the surface z. The local density of fluid molecules, however, depends also on the orientation of molecules with respect to the surface. Following refs 18, 26, and 32, we introduce the orientation distribution function $\alpha(\mathbf{r}, \hat{\mathbf{u}}_f) \equiv \alpha(\mathbf{r}, \omega)$ in the following way

$$\rho(\mathbf{r}, \omega) = \tilde{\rho}(\mathbf{r})\alpha(\mathbf{r}, \omega) \qquad (16)$$

In the above, $\omega = (\phi, \theta)$; θ is the angle measured with respect to the positive direction of the OZ axis; and ϕ is the angle in the OXY plane. The function $\alpha(\mathbf{r}, \omega)$ is normalized, i.e.

$$\int d\omega \alpha(\mathbf{r}, \omega) = \int_0^{2\pi} d\phi \int_0^{\pi} d\theta \sin\theta\alpha(\mathbf{r}, \omega) = 1 \qquad (17)$$

The system is studied in a grand canonical ensemble with the constraint of constancy of the number of chain molecules, i.e.

$$\rho_c = \int dz\rho_{sj}(z) \qquad (18)$$

where ρ_c is the number of chain molecules per area of the surface; i.e., it is the surface density of the chains. Of course, the integral in eq 18 does not depend on the segment index j.

The thermodynamic potential appropriate to the description of the system is

$$\Omega = F[\{\rho_{sj}(\mathbf{r})\}, \rho(\mathbf{r}, \omega)] + \int d\mathbf{r}d\omega v(z, \hat{\mathbf{u}})\rho(\mathbf{r}, \hat{\mathbf{u}})$$
$$- \mu \int d\mathbf{r}\tilde{\rho}(\mathbf{r}) + \sum_{j=1}^{M} \int d\mathbf{r}\rho_{sj}(\mathbf{r})v_{sj}(z) \qquad (19)$$

where $F[\rho_s(\mathbf{r}), \rho(\mathbf{r})]$ is the Helmholtz free energy functional, and μ is the chemical potential of the fluid.

At the first stage, the free energy functional is expressed as the sum of ideal, F_{id}, and excess, F_{ex} terms, $F = F_{id} + F_{ex}$. The ideal term is known exactly (cf. refs 18, 32, 44−48, and 52)

$$F_{id}/kT = \int d\mathbf{r}\tilde{\rho}(\mathbf{r})[\ln(\tilde{\rho}(\mathbf{r})) - 1]$$
$$+ \int d\mathbf{r}d\omega\tilde{\rho}(\mathbf{r})\alpha(\mathbf{r}, \hat{\mathbf{u}})\ln[4\pi\alpha(\mathbf{r}, \hat{\mathbf{u}})]$$
$$+ \frac{1}{kT}\int d\mathbf{R}\rho^{(c)}(\mathbf{R})V_b(\mathbf{R}) + \int d\mathbf{R}\rho^{(c)}(\mathbf{R})$$
$$[\ln\rho^{(c)}(\mathbf{R}) - 1] \qquad (20)$$

Then, the excess free energy is divided into the contributions due to hard sphere interactions, Fhs, the contribution due to connectivity of chains, F_c, and the contribution from the anisotropic interparticle interactions. The contribution F_{hs} is evaluated according to the fundamental measure theory,[52] while the chain connectivity contribution, F_c, results from the first-order perturbation theory of Wertheim.[53] These contributions are given by eqs 7, 10, and 12 in ref 54, and for the sake of brevity we have included them in the Supporting Information. Note that none of the free energy contributions, F_{hs}, nor F_c depends on $\alpha(\mathbf{r}_1, \omega)$.

Finally, the anisotropic interactions between fluid molecules and fluid molecules and segments of the chain are described using the mean field approximation. The interactions between a fluid molecule and different segments, $j = 1, 2, ..., M$, of a chain may be, in general, different. The mean-field free energy term, $F_{att,MF}$ consists of two contributions, $F_{att,MF} = F_{att,MF}^{ff} + F_{att,MF}^{fj}$, where the first term is due to the fluid−fluid and the second term is due to the fluid−segments interaction. For fluid−fluid contributions, we have (cf. refs 18 and 32)

$$F_{att,MF}^{ff} = \frac{1}{2}\int d\mathbf{r}_1 d\mathbf{r}_2 d\omega_1 d\omega_2 \tilde{\rho}(\mathbf{r}_1)\tilde{\rho}(\mathbf{r}_2)\alpha(\mathbf{r}_1, \omega_1)\alpha(\mathbf{r}_2, \omega_2)U(r_{12})(\hat{\mathbf{u}}(\omega_1) - \hat{\mathbf{u}}(\omega_2))\cdot\hat{\mathbf{r}}_{21}$$
$$= \int d\mathbf{r}_1 d\mathbf{r}_2 d\omega_2 \tilde{\rho}(\mathbf{r}_1)\tilde{\rho}(\mathbf{r}_2)\alpha(\mathbf{r}_2, \omega_2)U(r_{12})\hat{\mathbf{u}}(\omega_2)\cdot\hat{\mathbf{r}}_{12} \qquad (21)$$

whereas the fluid−segment contribution is given by

$$F_{att,MF}^{fj} = \sum_{j=1}^{M} \int dr_1 dr_2 d\omega_2 \rho_{sj}(r_1) \tilde{\rho}(r_2) \alpha(r_2, \omega_2) U_{fj}(r_{12}) \hat{u}(\omega_2)$$

$$\cdot \hat{r}_{12} \tag{22}$$

When the interactions of fluid molecules with all the segments are the same, then all the terms of the sum 22 become identical; therefore, the summation operator can be removed, and the segment local densities $\rho_{sj}(r)$ should be replaced by the total segment density, $\rho_s(r)$.

The equilibrium density profiles are found by minimization of the thermodynamic potential Ω. Thus[55]

$$\frac{\delta\Omega}{\delta\rho^{(c)}(R)} = 0 \tag{23}$$

$$\frac{\delta\Omega}{\delta\tilde{\rho}(r)} = 0 \tag{24}$$

$$\frac{\delta\Omega}{\delta\alpha(r, \omega)} = 0 \tag{25}$$

After substituting eqs 20, 21, and 22 into eq 19 from eq 25 we obtain

$$\alpha(r_1, \omega) = \frac{\exp[a(r_1) \cdot \hat{u}(\omega)]}{\int d\omega \, \exp[a(r_1) \cdot \hat{u}(\omega)]} \tag{26}$$

where

$$a(r_1) = \beta \Big[\int dr_2 \tilde{\rho}(r_2) U(r_{12}) \hat{r}_{12} + \sum_{j=1}^{M} \int dr_2 \rho_{sj}(r_2) U_{fj}(r_{12}) \hat{r}_{12}$$

$$- v^A(z) \hat{e}_z \Big] \tag{27}$$

To derive the equations for $\rho_{sj}(z)$ and $\tilde{\rho}(z)$, we make use of eqs 20, 21, 22, 26, and 27 and rewrite eq 19 as follows

$$\Omega = kT \int dR \rho^{(c)}(R)[\ln \rho^{(c)}(R) - 1]$$

$$+ \int dR \rho^{(c)}(R) V_b(R) + kT \int dr \tilde{\rho}(r)[\ln \tilde{\rho}(r) - 1]$$

$$+ \sum_{j=1}^{N} \int dr \rho_{sj}(r) v_{sj}(z) + \int dr \tilde{\rho}(r) v^{HW}(z)$$

$$- \mu \int dr \tilde{\rho}(r) + F_{hs} + F_c - F_a \tag{28}$$

where

$$F_a = kT \int \tilde{\rho}(r) \ln\left[\frac{\sinh(|a(r)|)}{|a(r)|}\right] \tag{29}$$

Then, from eqs 24 and 28 we obtain

$$\tilde{\rho}(z) = \exp\left\{\beta\left[\mu - v^{HW}(z) - \frac{\delta[F_{hs} + F_c]}{\delta\tilde{\rho}(z)} + \frac{\delta F_a}{\delta\tilde{\rho}(z)}\right]\right\} \tag{30}$$

The expressions for the functional derivative $\delta[F_{hs} + F_c]/\delta\tilde{\rho}(z)$ can be found in refs 44−48, 52, and 54, while the functional derivative $\delta F_a/\delta\tilde{\rho}(z)$ is calculated as

$$\frac{\delta F_a}{\delta\tilde{\rho}(z)} = \ln\left[\frac{\sinh(|a(r)|)}{|a(r)|}\right] + \int dr' \tilde{\rho}(r') U(|r - r'|)$$

$$\{[\tanh|a(r')|]^{-1} + [|a(r')|]^{-1}\}\frac{a(r') \cdot \hat{e}_z}{|a(r')|} \tag{31}$$

The evaluation of the density profiles of segments, $\rho_{sj}(r)$, is more complicated. To do that we follow the equations of refs 44−48, 52, and 54. The result is

$$\rho_{sj}(z) = \mathcal{W} \exp[-\beta\lambda_j(z)] G_j^{(L)}(z) G_{M-i+1}^{(R)}(z) \tag{32}$$

where the constant $\widetilde{\mathcal{W}}$ results from the normalization condition, eq 18, and

$$\lambda_j(z) = \frac{\delta[F_{hs} + F_c]}{\delta\tilde{\rho}(z)} + v_{sj}(z) + \int dr' \tilde{\rho}(r') U_{fj}(|r - r'|)$$

$$\{[\tanh|a(r')|]^{-1} + [|a(r')|]^{-1}\}\frac{a(r') \cdot \hat{e}_z}{|a(r')|} \tag{33}$$

The functions $G_j^{(L)}(z)$ and $G_j^{(R)}(z)$ are determined from the recurrence relation

$$G_i^{(L)}(z) = \int dz' \, \exp[-\beta\lambda_{i-1}(z')]\frac{\Theta(\sigma_c - |z - z'|)}{2\sigma_c} G_{i-1}^{(L)}(z') \tag{34}$$

and

$$G_i^{(R)}(z) = \int dz' \, \exp[-\beta\lambda_{M-i+2}(z')]$$

$$\frac{\Theta(\sigma_c - |z - z'|)}{2\sigma_c} G_{i-1}^{(R)}(z') \tag{35}$$

for $i = 2, 3, ..., M$ and with $G_1^{(L)}(z) = G_1^{(R)}(z) \equiv 1$. In the above $\Theta(s - x)$ is the step function.

Equations 26, 30, and 32 summarize our development. The solution of these equations with respect to the density profiles $\tilde{\rho}(z)$ and $\rho_{sj}(z)$ and the orientation profile $\alpha(z, \theta)$ was based on the Piccard iteration scheme, and all the convolutions were determined employing the Fast Fourier Transform subroutines from the FFTW library.[56,57] This method is quite standard now, and all numerical details can be found in the paper of Roth.[58] However, in the case of the system under study, one should pay special attention to the integrands in eq 31. It has been already noted by Rosenthal[18] that for very low local densities it is necessary to calculate the limiting values

$$\lim_{|a(r)| \to 0} \frac{\sinh(|a(r)|)}{|a(r)|} = 1 \tag{36}$$

and

$$\lim_{|a(r)| \to 0} \{[\tanh|a(r')|]^{-1} + [|a(r')|]^{-1}\} = 0 \tag{37}$$

and then to incorporate these into eq 31 with additional clauses.

To characterize the structure of the adlayer, it is also useful to introduce the orientation order parameter

$$h(z) = 2\pi \int_0^\pi d\theta \, \sin\theta \, \alpha(z, \theta) \cos\theta \tag{38}$$

The function $h(z)$ describes the "polarization" of the particles. It can take values between −1 and 1 corresponding to the

1169

dx.doi.org/10.1021/jp3105979 | J. Phys. Chem. B 2013, 117, 1166−1175

complete alignment of the Janus spheres in negative (positive) z-direction at a given value of z.

■ RESULTS AND DISCUSSION

The system in question is characterized by numerous parameters. To reduce their number, we assume that all spherical species (i.e., fluid particles and segments) have the same size, $\sigma_c = \sigma$. We also assume that all the segments are characterized by the same values of the parameters C_{fj} and λ_{fj} and that $\lambda_{fj} = \lambda = 3\sigma$. The reduced temperature is defined as $T^* = kT/C$. Moreover, σ is taken as the unit of length; so the reduced distance is $z^* = z/\sigma$, and the reduced densities are $\rho^*(z) = \rho(z)\sigma^3$ and $\rho_{sj}^*(z) = \rho_{sj}(z)\sigma^3$.

The parameters that characterize the brush are the number of segments, M, and the surface brush density, $R_c = \rho_c \sigma^2$. The calculations are carried out for rather short chains, $M = 2$ and $M = 6$.

The calculations carried out by Tarazona et al.[26] indicated that for a bulk system the present model predicts the formation of not only planar structures ("membrane-like") but also spherical structures ("vesicles"). In the case of the systems under study, i.e., in the presence of adsorbing walls, a full, three-dimensional calculation would be difficult. Therefore, we have limited ourselves to study the cases of density distributions with the symmetry resulting from the presence of the walls and assume translational symmetry in the other spatial dimensions. Consequently, the orientation distribution also simplifies to $\alpha(\mathbf{r}, \boldsymbol{\omega}) = \alpha(z, \theta)$.

The bulk (reference) fluid is the one-component fluid involving Janus particles. When a mean-field theory is used to describe a disordered bulk fluid, the quantity $|\alpha|$ is zero. Thus, for a disordered bulk system, the mean-field pressure and chemical potential are just the same as for the system of hard spheres. We can characterize the bulk disordered fluid either by the value of the chemical potential, μ, or by its density, ρ_b, $\rho_b^* = \rho_b \sigma^3$.

When only a planar symmetry is considered, the bulk system exhibits a continuous transition from a disordered to membrane-like structure. Performing calculations analogous to those of refs 26 and 32, we have found the phase diagram very close to that reported by Tarazona et al.[26] Small differences can be attributed to different treatments of the hard-sphere contributions to the free-energy functional in both approaches. All our model calculations have been carried out at a fixed temperature, $T^* = 0.2$. At that temperature the transition from a disordered to membrane-like structure in the bulk fluid occurs at $\rho_b^* \approx 0.248$.

We begin with the presentation of examples of adsorption isotherms $\Gamma^* = \Gamma \sigma^2$

$$\Gamma = \int dz[\tilde{\rho}(z) - \rho_b] \tag{39}$$

In Figure 2 we show a set of isotherms of Janus particles at $T^* = 0.2$ on nonmodified (the curves marked $R_c = 0$) and on modified ($R_c = 0.05$ and $R_c = 0.4$) surfaces. The surface is just a hard wall; i.e., the Yukawa potential energy parameter, C_{fs}, is zero. The brushes are built of $M = 2$ and $M = 6$ segments that are inert with respect to the Janus particles, $C_{fj} = 0$. Two surface densities of brushes, namely, $R_c = 0.05$ and $R_c = 0.4$, are considered. Due to structural transition in a bulk fluid, our calculations were carried out only for $\rho_b^* < 0.248$. For a comparison we have also displayed here adsorption isotherms of hard spheres, $C = 0$.
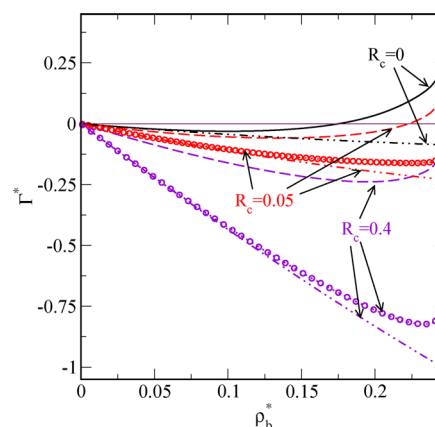

Figure 2. Adsorption isotherms of Janus particles at $T^* = 0.2$ on nonmodified and modified surfaces. The values of R_c are given in the figure; the curves labeled $R_c = 0$ are for a nonmodified surface. Dashed lines are for $M = 2$ and dotted lines with circles for $M = 6$. Dash-dotted lines denote adsorption isotherms of hard spheres. In the case of hard spheres the length of attached chains was $M = 6$.

In general, the excess adsorption isotherms are negative. Exceptions, but only at higher bulk fluid densities, are the isotherms of Janus particles on the nonmodified surface and on the surface modified with the chains of $M = 2$ at low surface grafting density, $R_c = 0.05$. Because of lack of attractive forces between the segments of chains and fluid molecules, the brush acts as a set of obstacles, and therefore covering the surface with a brush leads to lowering the adsorption. A more pronounced effect occurs for longer chains and for larger grafting densities, R_c.

Positive adsorption of Janus particles on a nonmodified surface at higher bulk densities results from a specific orientation of molecules within the adlayer adjacent to the surface; cf. Figures 3a and 3b where we have displayed the examples of the density profiles (Figure 3a) and examples of the orientation order parameter, $h(z)$ (Figure 3b). Note that the contact (i.e., at $z^* = 0.5$) values of the density profiles for Janus particles and for hard spheres are the same. This results from the theorem that the contact value of the density profile is related to the bulk pressure.[59] Within the considered model the bulk pressures of hard spheres and of disordered bulk Janus fluid are identical.

The orientation of a pair of particles is the most energetically favorable, when $(\hat{\mathbf{u}}_1 - \hat{\mathbf{u}}_2)\cdot\hat{\mathbf{r}}_{21} = -2$ (cf. Figure 1b). A "membrane"-like structure at the wall is built when the particles in vicinity of the wall expose their "hydrophilic" parts to the solid surface, i.e., when $\theta = \pi$. Within the first two layers, the Janus particles start to form a more packed structure in which the particles agglomerate (Figures 3a and 3b). Several first layer particles face their "hydrophilic" parts to the wall. The particles located at larger distances from the wall, however, assume an inverse orientation. From the values of the function $h(z)$ plotted in Figure 3b for a nonmodified surface (thick solid line) at the first minimum and at the first maximum, it appears that the average orientation of the particles adjacent to the wall is close to $2\pi/3$, while the angle for the second layer particles is close to $4\pi/9$. For a better visualization, we have schematically drawn representative first and second layer particles, whose orientations correspond to the average values given above. Consequently, there is an effective attraction between particles
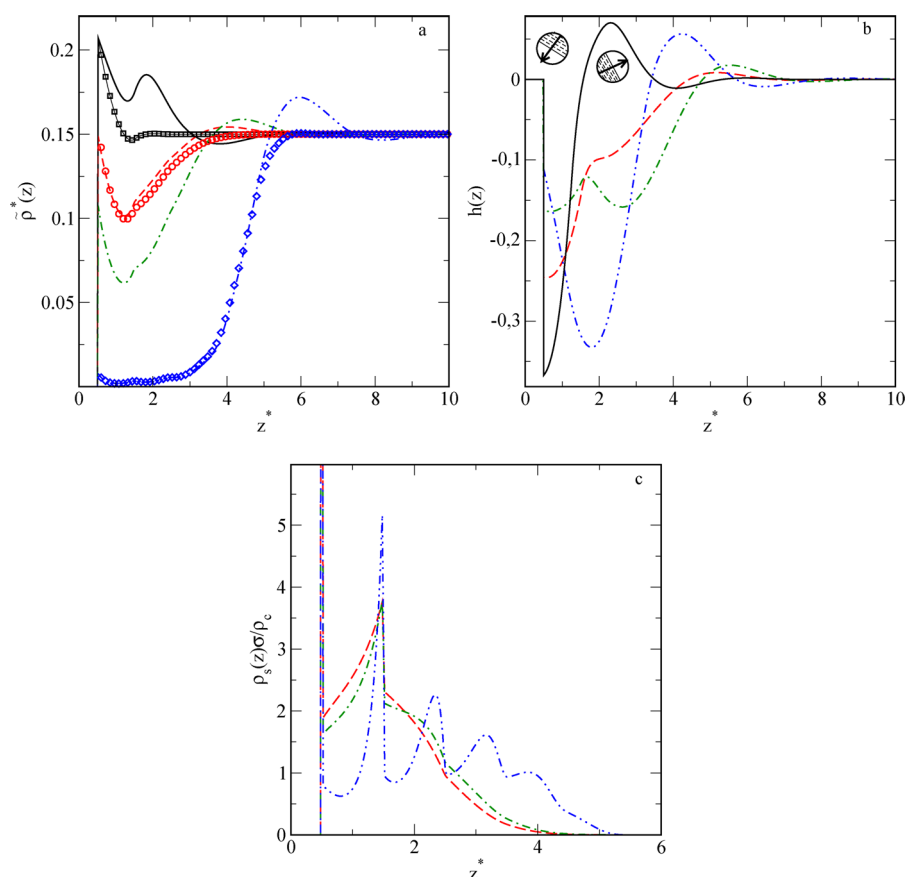
Figure 3. (a) Density profiles of Janus particles (lines) and of hard spheres (symbols). Solid line and squares are for nonmodified surface; dashed line and circles are for $M = 6$ and $R_c = 0.05$; dash-dotted line is for $M = 6$ and $R_c = 0.1$; and dash-double dotted line and diamonds are for $M = 6$ and $R_c = 0.4$. (b) The function $h(z)$ for systems from (a). The nomenclature of the lines is the same as in part a. We have also schematically drawn here the fluid molecules, whose orientations correspond to the average orientations within the first (at $z^* = 0.5$) and the second (at $z \approx 1.6$) adlayers. (c) The total segment density profiles for systems involving Janus particles from (a). The nomenclature of the lines is the same as in part a. In all parts the bulk fluid density is $\rho_b^* = 0.15$, and the temperature is $T^* = 0.2$.
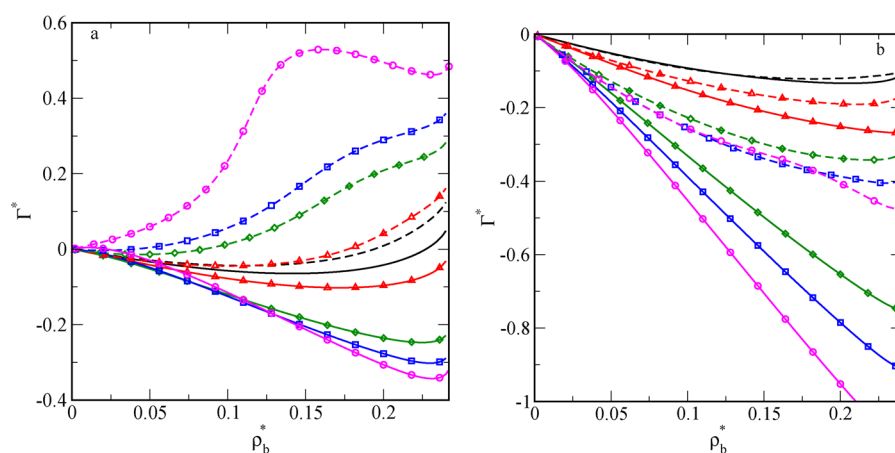

Figure 4. Adsorption isotherms on a surface modified with tethered chains built of $M = 2$ (part a) and $M = 6$ (part b) segments. Lines without symbols are for $R_c = 0.05$, decorated with triangles are for $R_c = 0.1$, with diamonds for $R_c = 0.3$, with squares for $R_c = 0.4$, and with circles for $R_c = 0.6$. Solid lines are for $C_{fj} = C$, while dashed lines are for $C_{fj} = -C$. The temperature is $T = 0.2$.

located within the surface layer that causes the adsorption increase, in comparison to the adsorption of hard spheres.

The presence of tethered chains that act like obstacles causes the fluid molecules to be expelled from the surface region. This effect is the most pronounced for $M = 6$ and $R_c = 0.4$, where the local density of fluid densities within the tethered layer drops

almost to zero (Figure 3a). Instantaneously, when the grafting density R_c increases, an "outer" part of the tethered layer acts as a "new" adsorbing surface, and an accumulation of the fluid particles within that region is observed. An increase of R_c causes the orientation ordering of the fluid particles located within the tethered layer to diminish first, but then it starts to increase
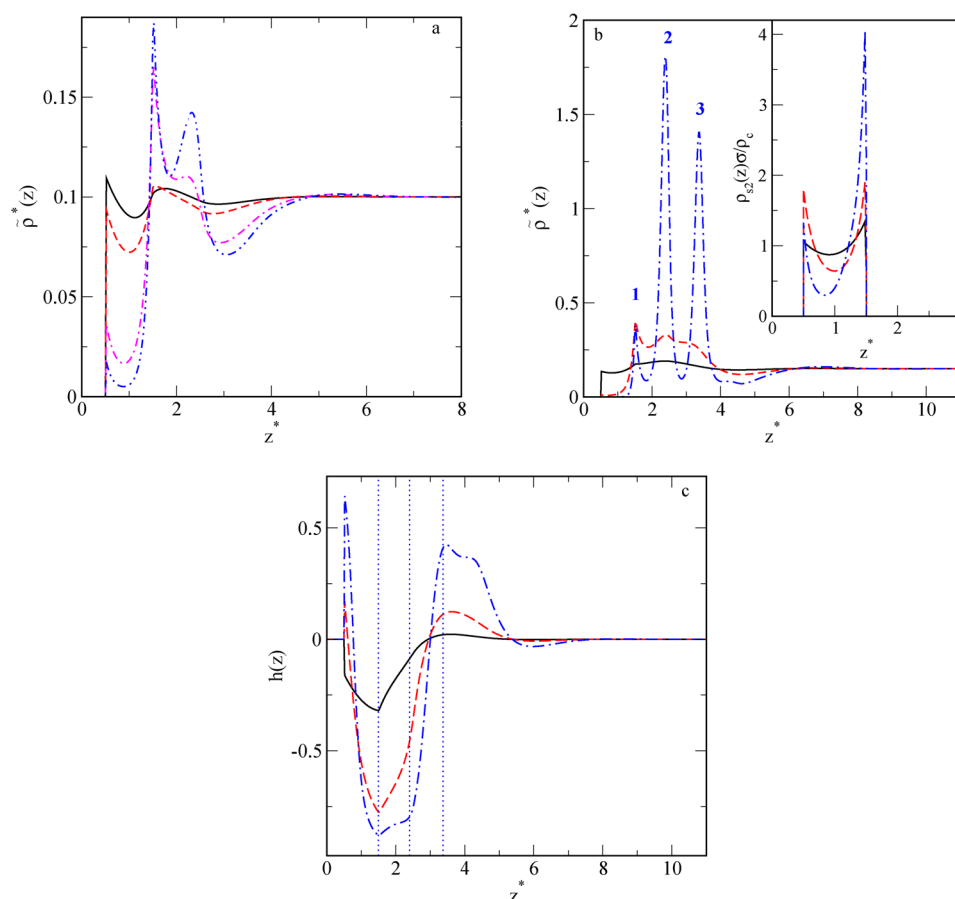
Figure 5. (a and b) Fluid density profiles. The chains are built of $M = 2$ segments. The bulk density is $\rho_b^* = 0.1$. The temperature is $T^* = 0.2$. In part (a) grafting densities are: 0.05 (solid line); 0.1 (dashed line); 0.3 (dash-dotted line); and 0.4 (dash-double dotted line). The segment−fluid interaction parameter is $C_{fj} = C$. In part b, the grafting densities are: $R_c = 0.05$ - solid line; $R_c = 0.3$ - dashed line; and $R_c = 0.6$ - dash-dotted line. The inset shows the local densities of the second segment, $\rho_{S2}(z)$, normalized by the grafting density. Part c shows the functions $h(z)$ for the systems from part b (the nomenclature of the lines is the same as in part b). Dotted vertical lines indicate the positions of the consecutive maxima, labeled by 1, 2, and 3 in part b.

(Figure 3b). However, the number of such particles is much smaller than for the nonmodified surface because the presence of the segments of the brush within that region reduces the space available to fluid particles (Figures 3a and 3c). Indeed, for higher values of R_c a well-ordered structure of the brush develops (Figure 3c), and for $R_c = 0.4$ the amount of fluid molecules within the region of $z^* < 4$ is very low (see Figure 3a).

Lower adsorption on modified surfaces is due to a depletion of the fluid density profiles within the region occupied by brush molecules (Figure 3a). Because of the lack of attractive forces between the segments of chains and fluid molecules, the brush acts as a set of obstacles, and therefore the lowest adsorption is observed for longer chains and for larger surface grafting densities, R_c. The adsorption of Janus particles is higher than the adsorption of hard-spheres, however. This is due to the effective attraction between adsorbed adlayers.

We now consider the case when the segments of grafted chains interact with fluid species, $C_{fj} \neq 0$. Two cases are considered, namely, $C_{fj} = C$ and $C_{fj} = -C$. In both cases, the magnitude of the Yukawa energy parameter for segment−fluid interactions is the same. In the first case, $C_{fj} = C$, the segments attract "hydrophobic" parts of Janus particles; i.e. they "act" against the formation of aggregates within the fluid. In the second case, however, they may "stimulate" formation of

aggregates. The interaction of fluid molecules with the "bare" surface is still of a hard-wall type.

In Figure 4, we present the adsorption isotherms for the systems with $M = 2$ (part a) and with $M = 6$ (part b). In both cases the calculations were carried out for the systems with $C_{fj} = C$ and $C_{fj} = -C$ and for different grafting densities. When the grafted chains are very short ($M = 2$), the system behaves like a heterogeneous surface with randomly distributed sites. The interaction of fluid molecules with those sites can either enhance ($C_{fj} = -C$) or inhibit the formation of aggregates (or a membrane-like structure, when the density is sufficiently high). There is an interplay between the volume exclusion effects and orientation-dependent segment−fluid molecule forces. For short chains, the latter effect prevails, and we observe a significant increase of adsorption (for $C_{fj} = -C$) and a pronounced decrease of adsorption (for $C_{fj} = C$) in comparison to the systems, in which the segments of tethered molecules act as obstacles (cf. Figure 4a).

If $C_{fj} = -C$, the interactions between segments of short chains and fluid particles "help" form the aggregates between fluid molecules. Consequently, the adsorption increases. An opposite effect is observed for $C_{fj} = C$. Now, the segment−fluid interactions compete with fluid−fluid interactions, destroying a possibility to form aggregates between fluid molecules.
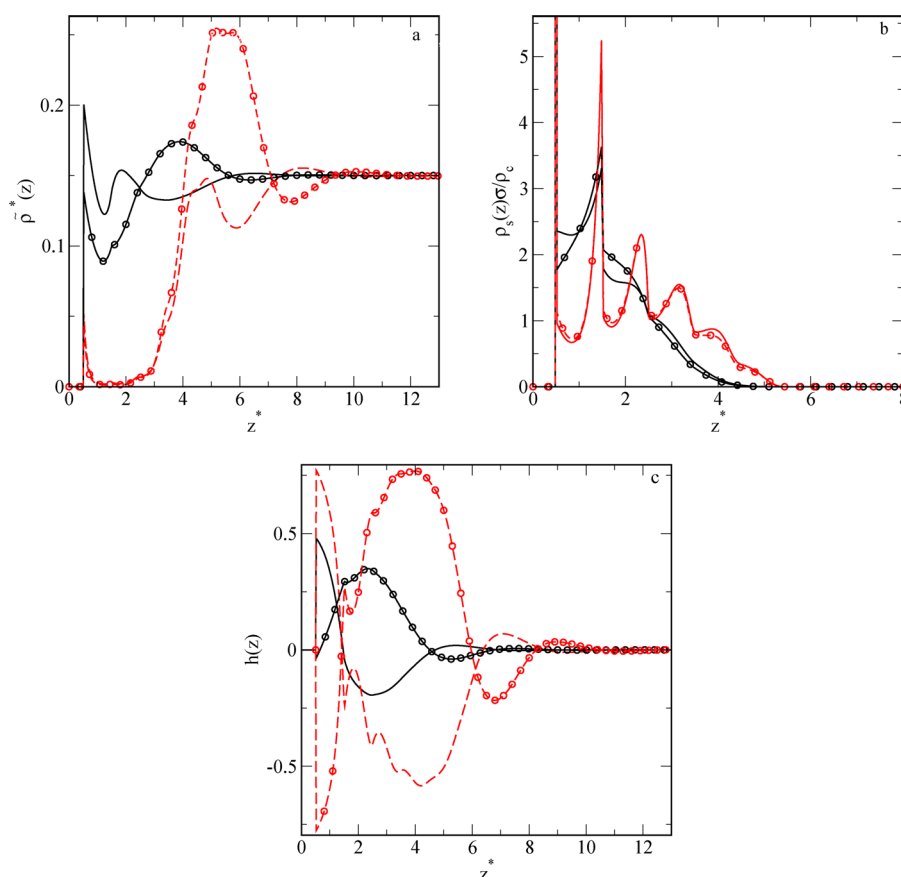
Figure 6. Fluid density profiles (part a), total segment density profiles (part b), and the functions $h(z)$ for the system with grafted hexamers at the two grafting densities, $R_c = 0.05$ (solid lines) and $R_c = 0.4$ (dashed lines). Lines without symbols are for $C_{fj} = C$, whereas lines with symbols are for $C_{fj} = -C$. The bulk density is $\rho_b^* = 0.15$, and the temperature is $T^* = 0.2$.

Consequently, the adsorption decreases, and this decrease is more pronounced for larger grafting densities.

In Figures 5a and 5b, we show the structure of fluid particles for the two kinds of systems discussed above. Part a is for the case when the segment−fluid interactions "disturb a correct" orientation of fluid particles, while for the systems from Figure 5b, the segment−fluid interaction enhances the formation of a "membrane-like" structure within the adsorbed layer. When the grafting density, R_c, is high enough, the outer surface of the chains is sufficiently dense to create "a new wall" that exerts a force ordering the molecules. For $C_{fj} = -C$ the ordering enforced by segment−fluid interactions leads to an increase of attraction between fluid molecules in the vicinity of the surface and to an increase of adsorption. The phenomenon described above is seen in Figures 5b and 5c for $R_c = 0.6$. The fluid molecules form three-well pronounced layers (the consecutive layers are distinguished by the labels 1, 2, and 3). The height of the first local density peak is the smallest, but the maximum of this peak is at the $z^* = 1.5$, where the local density of the $j = 2$ segment also possesses its maximum (see the inset to Figure 5b). Figure 5c illustrates how the function $h(z)$ changes with a distance from the wall. The vertical dotted lines correspond to the positions of the local density peaks at $R_c = 0.6$ in Figure 5b (labeled 1, 2, and 3, respectively).

In the case of longer grafted chains (Figures 4b and 5b), the volume exclusion effect prevails, and the excess adsorption is negative for all the systems under study. For the system with $C_{fj} = -C$ the fluid particles accumulate at the outer part of the brush. This is particularly visible for larger grafting densities,

while for lower values of R_c the fluid molecules can penetrate the brush (see Figure 6a). However, the accumulation of fluid molecules within the outer part of the brush does not balance the expelling of the fluid molecules from the region close to the wall, and the resultant isotherm is negative. Of course, the structure of the brush not only changes with the grafting density, R_c, but also depends on the segment−fluid interactions (Figure 6b). In particular, accumulation of the fluid molecules at the outer part of the brush "pushes" the segments toward the wall. Consequently, the brush characterized by the value of the Yukawa parameter $C_{fj} = -C$ becomes slightly more compact in comparison with the brush, characterized by $C_{fj} = C$. In Figure 6c we display the functions $h(z)$ for the systems from Figure 6a. It is interesting that $h(z)$ for the system with $C_{fj} = C$ and for $R_c = 0.4$ exhibits the structure reflecting the positions of consecutive maxima and minima of the total segment density from Figure 6b. One should remember, however, that the density of fluid within that region is very small (cf. Figure 6a).

Finally, we have carried out calculations for the nonzero anisotropic part of the fluid−solid potential, $v^A(z)$, (cf. eq 7). Of course, depending on the orientation of fluid molecules enforced by the anisotropic fluid−solid potential, it can expect either enhancement or inhibition of the formation of ordered adlayers in the vicinity of the surface. Moreover, the fluid−solid anisotropic potential can act "in accordance" with or "against" the fluid−segment orientation forces. In addition, a change of the grafting density R_c, as well as the change of the length of tethered chains, can alter the volume exclusion effects, which can become more or less important. The structure of the

adsorbed fluid depends on an interplay between all those factors, and even a small change of some modeled parameters may result in a quite unexpected behavior. Unfortunately, a systematic study of the role of all the parameters of the model would require massive (and time-consuming) calculations. Therefore, the aim of our investigation was to illustrate some new possibilities that can emerge rather than to obtain a complete description of the model.

The transition from the disordered to membrane-like phase in the bulk fluid observed in refs 26 and 32 was continuous. However, one can expect that the presence of strong fluid–wall interactions can enforce a first-order transition. This point is illustrated in Figure 7a. We show here examples of adsorption
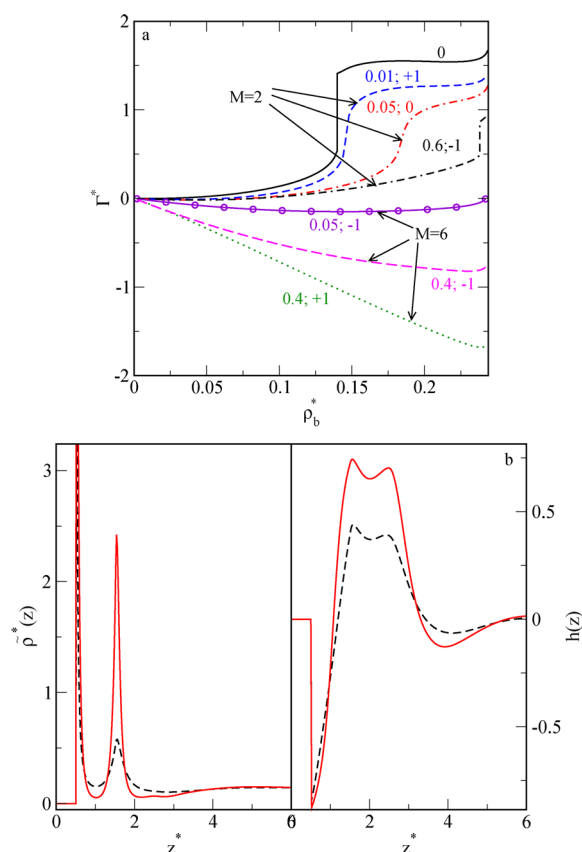
Figure 7. (a) Examples of adsorption isotherms. The pairs of numbers give the values of R_c and m, where m is given by $C_{fj} = mC$. The curve labeled O is for the nonmodified surface. Parts b and c show the density profiles just before (dashed lines) and after (solid lines) the transition that takes place at $\rho_b^* \approx 0.139$. All remaining parameters are given in the text.

isotherms for several selected systems. In all cases $C_{fs} = -C$. This potential "helps" the fluid molecules to assume the orientation that leads to the formation of a membrane at the wall. Moreover, we assumed that the range of the fluid–solid potential, $v^A(z)$, is two times longer than the range of all remaining anisotropic interactions, $\lambda_{fs} = 6\sigma$. For the non-modified surface, we observe a jump on the adsorption isotherm. This jump occurs at $\rho_b^* \approx 0.139$ and is connected with an abrupt formation of a bilayer (cf. Figures 7b and 7c). The occurring transition remains a layering transition in the systems involving Lennard-Jones fluids in contact with modified surfaces.[60]

The presence of even a small amount of pinned short ($M = 2$) destroys the transition, especially when $C_{fj} = +C$ (cf. Figure 7a, the curve abbreviated 0.01; + 1). However, for $M = 2$, $R_c = 0.6$, and for $C_{fj} = -C$, the first-order transition still exists but is shifted toward high bulk density that is very close to the bulk transition density ($\rho_b \approx 0.248$). In the latter case, the transition takes place at the "outer" plane of the brush. In the case of longer attached chains, $M = 6$, the excess adsorption is negative, and no traces of the occurrence of a transition have been found. In general, the effect of the chains on the layering transition is similar to that observed for Lennard-Jones fluids in contact with modified surfaces.[60,61]

In the case of adsorption of amphiphilic molecules on nonmodified and on modified surfaces, several interesting and novel phenomena can occur. We have studied here only the case of a planar symmetry. However, the development of a theoretical method that would include a possibility of formation of spherical self-assembled structures at the walls seems to be crucial for a complete description of such systems. Another open point is the vapor–liquid transition in the system. The present mean-field approach leads to cancellation of the anisotropic contribution to the functional in a homogeneous, isotropic state, and thus it does not lead to the gas–liquid transition in the bulk fluid. On the other hand, some preliminary results[32] obtained for the bulk system from the so-called modified mean-field bulk theory, according to which the pair correlation function is approximated by the Boltzmann factor, indicate that there exists such a transition. Thus, it seems to be also important to propose for nonuniform systems a modification of the theory that would more accurately describe the attractive force contribution to the free energy functional. The case of extremely small tethered molecules, composed just of one segment, seems also worth investigating. In such a way, one can modify the properties of the original surface by "attaching" to it randomly distributed centers that can change its properties, e.g., for "hydrophilic" to "hydrophobic" (or vice versa). All these problems are currently under study in our laboratories.

■ ASSOCIATED CONTENT

Ⓢ Supporting Information
Additional experimental details. This material is available free of charge via the Internet at http://pubs.acs.org.

■ AUTHOR INFORMATION

Corresponding Author
*E-mail: stefan.sokolowski@gmail.com.

Notes
The authors declare no competing financial interest.

■ ACKNOWLEDGMENTS

■ REFERENCES

(1) Casagrande, C.; Fabre, P.; Raphaël, E.; Veyssié, M. *Europhys. Lett.* **1989**, *9*, 251.
(2) de Gennes, P.-G. *Angew. Chem., Int. Ed.* **1992**, *31*, 842.
(3) Perro, A.; Reculusa, S.; Ravaine, S.; Bourgeat-Lami, E.; Duguet, E. *J. Mater. Chem.* **2005**, *15*, 3745.
(4) Vanakaras, A. G. *Langmuir* **2005**, *22*, 88.

(5) Pavlick, R. A.; Sengupta, S.; McFadden, T.; Zhang, H.; Sen, A. *Angew. Chem., Int. Ed.* **2011**, *50*, 9374.

(6) Ebbens, S. J.; Howse, J. R. *Langmuir* **2011**, *27*, 12293.

(7) Baraban, L.; Makarov, D.; Streubel, R.; Mänch, I.; Grimm, D.; Sanchez, S.; Schmidt, O. G. *ACS Nano* **2012**, *6*, 3383.

(8) Yin, S.-N.; Wang, C.-F.; Yu, Z.-Y.; Wang, J.; Liu, S.-S.; Chen, S. *Adv. Mater.* **2011**, *23*, 2915.

(9) Jiang, S.; Chen, Q.; Tripathy, M.; Luijten, E.; Schweizer, K. S.; Granick, S. *Adv. Mater.* **2010**, *22*, 1060.

(10) Grüschel, A. H.; Walther, A.; Löbling, T. I.; Schmelz, J.; Hanisch, A.; Schmalz, H.; Müller, A. H. E. *J. Am. Chem. Soc.* **2012**, *134*, 13850.

(11) Meng, X.; Guan, Y.; Zhang, Z.; Qiu, D. *Langmuir* **2012**, *28*, 12472.

(12) Schmid, F. In *Computational Methods in Surface and Colloid Science*; Borówko, M., Ed.; Marcel Dekker: New York, 2000; p 631.

(13) Marshall, B. D.; Emborsky, C.; Cox, K. R.; Chapman, W. G. *J. Phys. Chem. B* **2012**, *116*, 2730.

(14) Thompson, R. B.; Jebb, T.; Wen, Y. *Soft Matter* **2012**, *8*, 9877.

(15) Mondal, J.; Yethiraj, A. *J. Phys. Chem. Lett.* **2011**, *2*, 2391.

(16) Emborsky, C. P.; Feng, Z.; Cox, K. R.; Chapman, W. G. *Fluid Phase Equilib.* **2011**, *306*, 15.

(17) Vasilevskaya, V. V.; Ermilov, V. A. *Polym. Sci., Ser. A* **2011**, *53*, 846.

(18) Rosenthal, G. Theory and computer simulations of amphiphilic Janus particles, *PhD thesis*, TU Berlin, 2012, http://opus.kobv.de/tuberlin/volltexte/2012/3587/.

(19) Rosenthal, G.; Gubbins, K. E.; Klapp, S. H. L. *J. Chem. Phys.* **2012**, *136*, 174901.

(20) Jiang, S.; Granick, S. *J. Chem. Phys.* **2007**, *127*, 161102.

(21) Jiang, S.; Chen, Q.; Tripathy, M.; Luijten, E.; Schweizer, K. S.; Granick, S. *Adv. Mater.* **2010**, *22*, 1060.

(22) Sciortino, F.; Giacometti, A.; Pastore, G. *Phys. Chem. Chem. Phys.* **2010**, *12*, 11869.

(23) Lee, K. J.; Yoon, J.; Lahann, J. *Curr. Opin. Colloid Interface Sci.* **2011**, *16*, 195.

(24) Loget, G.; Kuhn, A. *J. Mater. Chem.* **2012**, *22*, 15457.

(25) Hagy, M. C.; Hernandez, R. *J. Chem. Phys.* **2012**, *137*, 044505.

(26) Somoza, A. M.; Chacón, E.; Mederos, L.; Tarazona, P. *J. Phys.: Condens. Matter* **1995**, *7*, 5753.

(27) Hong, L.; Cacciuto, A.; Luijten, E.; Granick, S. *Langmuir* **2008**, *24*, 621.

(28) Erdmann, T.; Kröger, M.; Hess, S. *Phys. Rev. E* **2003**, *67*, 041209.

(29) Guerra, C.; Somoza, A. M.; Telo da Gama, M. M. *J. Chem. Phys.* **1998**, *109*, 1152.

(30) Kern, N.; Frenkel, D. *J. Chem. Phys.* **2003**, *118*, 9882.

(31) Sciortino, F.; Giacometti, A.; Pastore, G. *Phys. Rev. Lett.* **2009**, *103*, 237801.

(32) Rosenthal, G.; Klapp, S. H. L. *J. Chem. Phys.* **2011**, *134*, 154707.

(33) Rosenthal, G.; Klapp, S. H. L. *Int. J. Mol. Sci.* **2012**, *13*, 9431.

(34) Naji, A.; Seidel, C.; Netz, R. R. *Adv. Polym. Sci.* **2006**, *198*, 149.

(35) Klushin, L. I.; Skvortsov, A. M. *J. Phys. A: Math. Theor.* **2011**, *44*, 473001.

(36) Binder, K.; Kreer, T.; Milchev, A. *Soft Matter* **2011**, *7*, 7159.

(37) Advincula, R. C.; Brittain, W. J.; Caster, K. C.; Rühe, J., Eds. *Polymer Brushes*; Wiley-VCH: Weinheim, 2004.

(38) Descas, R.; Sommer, J.-U.; Blumen, A. *Macromol. Theory Simul.* **2008**, *17*, 429.

(39) Garbassi, F.; Morra, M.; Occhiello, E. *Polymer surfaces: from physics to technology*; John Wiley & Sons: New York, 2002.

(40) Klein, J. *Science* **2009**, *323*, 47.

(41) Hucknall, A.; Rangarajan, S.; Chilkoti, A. *Adv. Mater.* **2009**, *21*, 2441.

(42) Wang, A. J.; Xu, J. J.; Chen, H. Y. *J. Chromatogr. A* **2007**, *120*, 1147.

(43) Li, Y.; Zhang, J.; Fang, L.; Wang, T.; Zhu, S.; Li, Y.; Wang, Z.; Zhang, L.; Cui, L.; Yang, B. *Small* **2011**, *7*, 2769.

(44) Borówko, M.; Patrykiejew, A.; Sokołowski, S. *J. Chem. Phys.* **2011**, *135*, 054703.

(45) Pizio, O.; Sokołowski, S.; Sokołowska, Z. *J. Chem. Phys.* **2011**, *134*, 214702.

(46) Borówko, M.; Patrykiejew, A.; Rżysko, W.; Sokołowski, S.; Ilnytskyi, J. *J. Chem. Phys.* **2011**, *134*, 044705.

(47) Borówko, M.; Patrykiejew, A.; Sokołowski, S.; Staszewski, T. *Collect. Czech. Chem. Commun.* **2010**, *75*, 221.

(48) Patrykiejew, A.; Sokołowski, S.; Tscheliessnig, R.; Fischer, J.; Pizio, O. *J. Phys. Chem. B* **2008**, *112*, 4552.

(49) Pizio, O.; Pusztai, L.; Sokołowska, Z.; Sokołowski, S. *J. Chem. Phys.* **2009**, *130*, 134501.

(50) Borówko, M.; Rżysko, W.; Sokołowski, S.; Staszewski, T. *J. Phys. Chem. B* **2009**, *113*, 4763.

(51) Borówko, M.; Sokołowski, S.; Staszewski, T. *J. Chromatogr A* **2011**, *1218*, 711.

(52) Yu, Y.-X.; Wu, J.-Z. *J. Chem. Phys.* **2002**, *117*, 2368−10156; **2003**, *118*, 3835.

(53) Wertheim, M. S. *J. Chem. Phys.* **1987**, *87*, 7323.

(54) Borówko, M.; Sokołowski, S.; Staszewski, T. *J. Colloid Interface Sci.* **2011**, *356*, 267.

(55) Evans, R. *Adv. Phys.* **1979**, *28*, 143.

(56) http://www.fftw.org (accessed January 14, 2013).

(57) Johnson, S. G., Frigo, M. *Implementing FFTs in Practice, in Fast Fourier Transforms*; Burrus, C. S., Ed.; Connexions: Houston, 2008; Chapter 11.

(58) Roth, R. *J. Phys.: Condens. Matter* **2010**, *22*, 063102.

(59) Lutsko, J. F. Recent Developments in Classical Density Functional Theory. In *Advances in Chemical Physics*; Rice, S.A., Ed.; John Wiley & Sons, Inc.: New York, 2010; Vol. *144*, pp 1−92.

(60) Sokołowska, Z.; Sokołowski, S. *J. Colloid Interface Sci.* **2007**, *316*, 652.

(61) Patrykiejew, A.; Sokołowski, S.; Tscheliessnig, R.; Fischer, J.; Pizio, O. *J. Phys. Chem. B* **2008**, *112*, 4552.